Journal of Materials Chemistry B

ROYAL SOCIETY OF CHEMISTRY

PAPER

View Article Online
View Journal | View Issue

Check for updates

Cite this: J. Mater. Chem. B, 2024, 12, 2083

A natural biogenic fluorapatite as a new biomaterial for orthopedics and dentistry: antibacterial activity of lingula seashell and its use for nanostructured biomimetic coatings†

Gabriela Graziani, ‡*[a] Daniele Ghezzi,*[ab] Fabio Nudelman,[c] Enrico Sassoni,*[d] Fraser Laidlaw,[e] Martina Cappelletti,[b] Marco Boi,[a] Giorgia Borciani,[a] Silvia Milita,[f] Michele Bianchi,[g] Nicola Baldini*[ah] and Giuseppe Falini*[i]

Received 18th October 2023,
Accepted 16th January 2024

DOI: 10.1039/d3tb02454g

rsc.li/materials-b

Calcium phosphates are widely studied in orthopedics and dentistry, to obtain biomimetic and antibacterial implants. However, the multi-substituted composition of mineralized tissues is not fully reproducible from synthetic procedures. Here, for the first time, we investigate the possible use of a natural, fluorapatite-based material, *i.e.*, *Lingula anatina* seashell, resembling the composition of bone and enamel, as a biomaterial source for orthopedics and dentistry. Indeed, thanks to its unique mineralization process and conditions, *L. anatina* seashell is among the few natural apatite-based shells, and naturally contains ions having possible antibacterial efficacy, *i.e.*, fluorine and zinc. After characterization, we explore its deposition by ionized jet deposition (IJD), to obtain nanostructured coatings for implantable devices. For the first time, we demonstrate that *L. anatina* seashells have strong antibacterial properties. Indeed, they significantly inhibit planktonic growth and cell adhesion of both Gram-positive *Staphylococcus aureus* and Gram-negative *Escherichia coli*. The two strains show different susceptibility to the mineral and organic parts of the seashells, the first being more susceptible to zinc and fluorine in the mineral part, and the second to the organic (chitin-based) component. Upon deposition by IJD, all films exhibit a nanostructured morphology and sub-micrometric thickness. The multi-doped, complex composition of the target is maintained in the coating, demonstrating the feasibility of deposition of coatings starting from biogenic precursors (seashells). In conclusion, Lingula seashell-based coatings are non-cytotoxic with strong antimicrobial capability, especially against Gram-positive strains, consistently with their higher susceptibility to fluorine and zinc. Importantly, these properties are improved compared to synthetic fluorapatite, showing that the films are promising for antimicrobial applications.

1. Introduction

Calcium phosphate (CaP)-based biomaterials have been widely studied for the development of bone substitutes and implant coatings to promote osseointegration and regeneration of native bone.[1–8] The widespread use of CaPs derives from their similarity to the mineral phase of bone, since, to boost osseointegration, a composition resembling as closely as possible that of mineralized tissues is desired.[9,10] However, together with promoting integration, implantable materials shall discourage infection, which is the main reason for implant failure in orthopedics and dentistry, and leads to severe complications.[11–13] The need for antibacterial solutions is becoming increasingly important, as the progressive development of micro- and nano-texturing and of custom-made porous 3D printed implants, aiming at creating multi-scale

[a] Biomedical Science, Technologies, and Nanobiotecnology Lab, IRCCS Istituto Ortopedico Rizzoli, Bologna, Italy. E-mail: gabriela.graziani(at)polimi.it
[b] Department of Pharmacy and Biotechnology, University of Bologna, Bologna, Italy
[c] EaStCHEM School of Chemistry, The University of Edinburgh, Edinburgh, UK
[d] Department of Civil, Chemical, Environmental and Materials Engineering, University of Bologna, Bologna, Italy
[e] School of Physics and Astronomy, The University of Edinburgh, Edinburgh, UK
[f] CNR-Institute for Microelectronic and Microsystems, Bologna, Italy
[g] Department of Life Sciences, Università di Modena e Reggio Emilia, Modena, Italy
[h] University of Bologna, Department of Biomedical and Neuromotor Sciences, Bologna, Italy
[i] Department of Chemistry "Giacomo Ciamician", University of Bologna, Bologna, Italy. E-mail: giuseppe.falini(at)unibo.it

† Electronic supplementary information (ESI) available. See DOI: https://doi.org/10.1039/d3tb02454g

‡ Present address: Department of Chemistry, Materials and Chemical Engineering "G. Natta", Politecnico di Milano, Milan, Italy.

topographical cues to promote cell attachment, proliferation and regeneration, also tends to favor bacterial adhesion. To this aim, functionalization of CaPs with antibacterial metals and/or drugs has been proposed.[14–19]

However, mineralized tissues are composed of multi-substituted calcium phosphates that cannot be reproduced from synthetic processes.[20,21] More specifically, bone, enamel and dentine apatite contain substitutions in the crystal lattice by carbonate, magnesium, fluorine, strontium, sodium, chlorine, potassium, silicates, zinc and manganese ions, in variable concentrations. Each trace ion has an impact on the characteristics of the crystal lattice, affecting the solubility and crystallinity of the material, and its interactions with the host.[9,20,25–43] In addition, some ions have specific therapeutic functions, including a concentration-dependent capability to inhibit microbial proliferation.[22–24]

Among trace ions present in human mineralized tissues, fluorine and zinc show a particularly promising behavior. Indeed, different from all the other substitutions (except for Sr at high concentrations), F^- substitution for OH^- causes an increase in the symmetry of the lattice, so that fluorine-substituted apatite shows higher stability and lower solubility than hydroxyapatite (HA). Notably, fluorine is expected to exert a positive influence against osteoporosis and to have antibacterial effect.[44] For these reasons, research on fluorine-substituted hydroxyapatite is attracting increasing attention for its use as bioactive and antibacterial material. Zinc also shows a high antibacterial effect if used at proper concentrations.[20,22]

To pursue biomimetism and exploit the biological role of different ions, research is moving towards the use of multi-doped apatites.[13,22,45–49] This is particularly important for infections, where different metal ions can inhibit different microbial populations, thus multi-doped apatites can be more effective than single-doped ones towards a larger number of bacterial strains.[50] However, obtaining multi-doped apatites is challenging, as each substitution causes distortion in the lattice, thus modifying the amount of other ions that can be entrapped. This becomes even more challenging when switching from bulk materials to coatings, where the capability of the technique to preserve the composition from the deposition target to the coating must also be taken into account. For this reason, the use of naturally derived biomaterials is being widely pursued and the deposition of coatings from biogenic sources to achieve multi-substituted coatings, and in particular that of bone, is raising increasing interest.[51–57]

Deposition of targets from biogenic sources to obtain nanostructured and adhesive films has been explored by pulsed laser deposition, magnetron sputtering and pulsed electron deposition.[58–61] In this regard, the authors have demonstrated that nanostructured thin films having a composition perfectly resembling that of the deposition target can be achieved by ionized jet deposition (IJD). Thanks to their nanostructured surface and the high surface area, high ion release is obtained, permitting a sustained antimicrobial activity.[62–65] At the same time, the combination of biomimetic composition and nanostructured morphology permits mitigation of toxicity towards host cells and in some cases can promote differentiation towards an osteogenic lineage.[58,59,64]

Together with the use of bone, biomaterials derived from seashells are also raising increasing interest. Seashells are a byproduct of the food industry, so their re-use for high added value applications is very promising in the view of circular economy and the use of sustainable sources for materials production. In addition, they have high availability and unique properties, including that of being multi-doped, that make them particularly suitable for application in biomaterials.[66] Calcium carbonate-based biomaterials have been proposed using unprocessed seashells, and conversion of carbonate in calcium phosphates has been largely explored, for the development of biomimetic materials, although nanostructured coatings deriving from seashells are yet to be explored.[66]

Here, we propose the use of natural fluorapatite deriving from the shell of the brachiopod *Lingula anatina* as an antibacterial biomaterial, mimicking the composition of dentine and enamel, for orthopedics and dentistry. The *L. anatina* shell is an organic–inorganic composite material, where the inorganic phase is made of 4–8 nm crystals of carbonate-substituted fluorapatite in the form of francolite and comprises *ca.* 68% of the shell weight.[67,68] The organic fraction, which comprises the remaining 32% of the shell weight, is composed of proteins, glycosaminoglycans and chitin.[67,69,70] At the micron scale, the shell has a laminated structure made of alternating layers of predominantly organic and predominantly mineral phases. The *L. anatina* shell is of particular interest to orthopedics and dentistry, as its inorganic composition is close to that of bone and enamel, and it contains ion dopants (magnesium, zinc, sodium, manganese) that are important to promote bone regeneration but difficult to incorporate into synthetically produced hydroxyapatite.

The compositional features and antibacterial action of *L. anatina* are studied, for its use in the form of granulates, or nano/micro-powders, to be embedded in polymeric/ceramic scaffolds. Then, its deposition is investigated by IJD, to produce nanostructured biomimetic thin films.

The composition of the coatings is studied to investigate the capability of IJD to preserve the main phase and the substitutions that are present in *L. anatina* seashell. Then, nanostructured morphology is shown and antibacterial action of the films is verified against Gram-positive and Gram-negative bacterial strains, for application in orthopedics, dentistry and maxillofacial surgery.

2. Experimental

2.1. Materials

L. anatina dry seashells (unprocessed) were used for the tests. The sample was supplied by the Mostra Mondiale Malacologia (Cupra Marittima, AP, Italy) and it was collected in the Salu Sea (Philippines).

Films were deposited onto titanium–aluminum–vanadium microstructured disks and on glass slides, after cleaning in

ethanol and water. Silicon wafers (Si) (p-type doped monocrystalline (100) native silicon, size 5 × 5 mm, thickness 1 mm, Fondazione Bruno Kessler, Trento, Italy) were also used as reference substrate for topographical characterizations. No surface preparation was carried out for any of the substrates, prior to deposition.

Synthetic fluorapatite was used for comparison sake, synthesized as described in ref. 71

2.2. Methods

2.2.1. Characterization of *L. anatina* seashell. Prior to its deposition, composition and morphology of *L. anatina* seashell were characterized.

Morphology was studied by Field Emission Gun Scanning Electron Microscopy (FEG-SEM, Tescan Mira3, CZ, working distance = 10 mm, voltage = 10 kV). FEG-SEM samples (fragments of lingula shell) were made conductive by sputtering with carbon before observation.

The mineralogical composition of *L. anatina* and its crystallinity were investigated by X-rays diffractometry (XRD, X'Pert PRO, Malvern Panalytical, Malvern, UK, 2θ = 5°–80°, scan step size 0.017°, time per step 50 s). Then, phase composition was also studied by Fourier transform infrared spectroscopy (FTIR-ATR, PerkinElmer Spectrum 2, acquisition parameters: resolution 1 cm^{-1}, accumulation 64 scans, data interval 0.5 cm^{-1}).

Both XRD and FT-IR were carried out on pulverized samples, obtained by manual grinding in agate mortar.

Elemental composition was tested by EDS and ICP (ICP-OES, Spectro Arcos-Ametek, Inductive Coupled Plasma Optical Emission Spectroscopy). For EDS, fragments of *L. anatina* shells were examined, without processing. The EDS analysis was performed using a Bruker probe coupled with the Tescan Mira 3 FEG-SEM. A working voltage of 10 kV was used and samples were made conductive by coating with carbon, as for the SEM observations. EDS spectra and maps were acquired to investigate distribution of calcium, phosphorous, zinc and fluorine in the shell. For ICP, after grinding, samples were digested in 4.5 mL ultrapure nitric acid and 0.5 mL hydrogen peroxide.

2.2.2. Antibacterial properties of lingula seashell. The antimicrobial activity of *L. anatina* was assessed against the two common human pathogens *E. coli* ATCC 8739 and *S. aureus* ATCC 6538P. The study was carried out by growing the bacterial cells in 50 mL tubes with 5 mL of Luria-Bertani (LB) liquid medium (NaCl 1%, tryptone 1%, yeast extract 0.5%) overnight at 37 °C under agitation at 130 rpm. For the tests, all the strains were diluted to reach an initial cellular concentration of 10^5 CFU mL^{-1}. The assays were performed in 12-well microplates with 1 mL of LB as growth medium. Around a quarter of the lingula (around 1.2 cm^2) was added to the cultures. The incubation was performed at 37 °C and 130 rpm. Bacterial cell enumeration was based on serial dilution method (using 20-μL volume from each culture) that was performed every hour in saline solution (NaCl 0.85%) and using LB agar plates as growth medium for colony forming units (CFU) count. Control experiments consisted in bacterial cultures grown on LB medium without the lingula addition. Each experiment was repeated in triplicate. All results are reported as mean ± standard deviation (SD) calculated from three replicates. Statistical analysis was performed using one-way Anova test. Differences were considered significant when $p < 0.05$.

The Minimal Inhibitory Concentration of both *L. anatina* shell and fluorapatite (used as a benchmark) was determined by culturing each strain in 5 mL LB in 6-well microplates supplied with shell powder and fluorapatite powder at different concentrations. After 24 hours of growth, serial dilutions and CFU counts were performed on LB agar plates. The minimal inhibitory concentration (MIC) was determined as the lowest concentration that prevented microbial growth.

2.2.3. Coatings deposition. Coatings were obtained by ionized jet deposition (IJD, Noivion Srl, Rovereto, Italy), as schematized in Fig. 1. During the process, the target

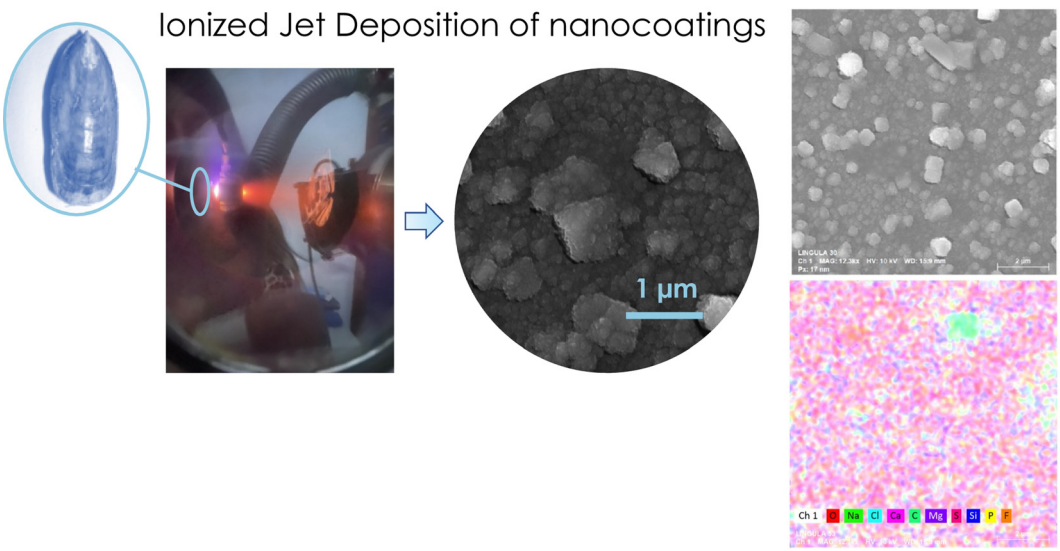

Fig. 1 IJD deposition scheme.

(unprocessed *L. anatina* seashell) is ablated by a fast pulse (100 ns) of high energy (10 J) and high-density (109 W cm^{-2}) electrons. Deposition parameters were selected based on (i) the uniformity of the plasma plume (possibility to obtain a plume at each pulse of the electron beam) and (ii) on preliminary data for deposition of calcium phosphates. As a consequence, the plasma plume was directed toward a substrate mounted at 8 cm distance from the target and a working voltage and an electron beam frequency of 17 kV and 7 Hz, respectively, were selected. Deposition time was set to 20 minutes, as it is the highest duration that can be achieved by using one target.

The deposition is carried out in vacuum (the chamber is initially evacuated down to a base pressure of 1.0×10^{-7} mbar by a turbomolecular pump – EXT255H, Edwards, Crawley, England), then pressure is raised by a controlled flow of oxygen up to 3×10^{-4} mbar. A *L. anatina* seashell was used as supplied, after washing in deionized water and ethanol and drying to constant weight. No processing of the shell was carried out to remove the organic components prior to deposition. For the deposition, one half of the shell was mounted on the target holder by using adhesive tape and used as a target.

2.2.3.1. Coatings morphology and composition. After deposition, morphology and composition of the coatings were studies to assess compliance to the objectives, *i.e.*, obtaining nanostructured and biomimetic thin films, having a composition as close as possible to that of the *L. anatina* seashell.

Coatings morphology was studied after deposition on titanium alloy disks, by FEG-SEM, as described above for the target. Based on FEG-SEM images at 50 000× magnification, the maximum and minimum dimension of the aggregates that constitute the films was measured by ImageJ software (National Institutes of Health, USA). To analyze the distribution in aggregates diameters, 3 non overlapping areas of two samples were selected, each composed by at least 45 clearly distinguishable aggregates. All areas had the same dimensions and were chosen within images at a 50 000× magnification.

Composition was investigated by FT-IR, EDS and ICP, as described above for the shell before deposition. Film composition by ICP and FT-IR is measured on silicon wafers.

Then on the coting 2D-GIWAXS images were collected at the XRD1 beamline of the ELETTRA Synchrotron radiation facility (Trieste, Italy), by using an incident X-ray beam of 1A and 200 × 200 μm^2 size and a 2D Pilatus detector placed at 90 cm from the sample position. The incident angle was fixed at α_i = 0.05 deg, 0.1 deg and 0.15 deg, to investigate different thickness of the samples, and moved laterally to probe different area of the sample.

2.2.3.2. Substrate effect on coatings properties. Coatings cross-section was also observed by FIB to study film thickness, morphology and presence/absence of pores and/or defects in the cross section. For FIB, coatings were deposited onto different materials, to study the impact of the substrate characteristics on coatings thickness and morphology. FIB milling and SEM imaging were done using a Zeiss Crossbeam 550 equipped with an inlens, secondary electrons, backscattered electrons detectors and an Oxford instruments energy-dispersive X-ray spectroscopy detector (EDS). Milling was done at an ion beam accelerating voltage of 30 kV and beam current of 7 nAmp, while SEM imaging was performed with an accelerating voltage of 5 kV using the inlens and backscattered electrons detector.

To assess the stability of the coatings, dissolution tests were performed in complete culture medium (sterile alpha-MEM, Minimum Essential Medium Eagle, Sigma Aldrich, supplemented with 1 wt% 100 U mL^{-1} penicillin and 100 μg mL^{-1} streptomycin to avoid bacterial contamination and 10% fetal bovine serum). Samples (2 for each timepoint) were submerged in medium at pH 7.4 for 24 h, 7 days, 14 days and 21 days, respectively. The desired pH was obtained by addition of $NaHCO_3$ (2.2 g l^{-1}). Films were placed in 24 wells and 1 ml medium was put into each well. Wells plates were sealed and kept in a humidified incubator at 37 °C, 95% air and 5% CO_2. Medium was refreshed every 72 h.

At each timepoint, stability was evaluated by observing samples morphology by SEM, performed as described above. SEM/EDS was performed on at least 2 non-overlapping areas of each sample, 1 close to the center and 1 on the samples edge.

The antimicrobial activity of deposited *L. anatina* seashell coatings was assessed by growing the microorganisms in 50 mL tubes with 5 mL of Luria-Bertani (LB) liquid medium (NaCl 1%, tryptone 1%, yeast extract 0.5%) overnight at 37 °C under agitation at 130 rpm. For the tests, all the strains were diluted to reach 10^5 CFU mL^{-1}. The assays were performed in 48-well microplates with 400 μL of LB medium. A glass piece 0.5 × 0.5 cm with deposited lingula shield on it was added to the cultures. The incubation was performed at 37 °C and 130 rpm. Serial dilutions of 20-μL of cultures were performed every hour in saline solution (NaCl 0.85%) and spread onto LB agar plates for CFU counting. Control experiments consisted in bacterial cultures with LB medium only. Each experiment was repeated in triplicate.

Biocompatibility of the coatings on glass slides was evaluated by measuring the cell viability of MG-63 osteoblast-like cells after the exposure to the coatings. For the test, 10×10^3 MG-63 were seeded at the bottom of a 48-well plate and the samples, previously sterilized under UV ray for 2 hours, were added at the well and placed in direct contact with cell monolayer, and maintained in culture for 7 days. Uncoated glass slides were used as control. Cell viability was monitored by Alamar Blue assay at 1, 3 and 7 days. Briefly, to perform Alamar Blue assay, the culture medium was removed, replaced with the Alamar Blue solution prepared as 10% v/v in fresh culture medium, then incubated at 37 °C, with 95% humidity for 3 h. The fluorescence was quantified in a microplate spectrophotometer (Infinite F200 PRO, TECAN, Mannedorf, Switzerland) at 535 nm excitation and 590 nm emission wavelengths. Data expressed as Relative Fluorescence Units (RFU), are reported as mean ± standard error of triplicates.

To exclude any potential toxic effect of the material's degradation by-products, the conditioned medium (CM), obtained

from keeping the samples in culture medium for 24 h, was added to previously seeded cell monolayer of MG-63 and maintained in culture for further 24 hours (37 °C, 95% humidity). The CM was diluted 100 : 0, 50 : 50, 25 : 75, and 5 : 95 with fresh culture medium. Cells cultured without administration of the conditioned medium were used as control.

3. Results & discussion

3.1. Characterization and antimicrobial efficacy of lingula shell

XRD spectra of *L. anatina* seashell are reported in Fig. 2. All peaks correspond to fluorapatite (JCPDS 15-0876), with a high crystallinity.[72] EDS data (Table 1 and Fig. S2, ESI†) show the presence of fluorine at an approximate concentration of 0.06 wt%, a calcium to phosphate ratio of 1.75 and the presence of Mg and Na ions. Elemental composition, as assessed by ICP (Table 2), shows that, together with fluorine, many elements are present in the shell, including magnesium, sodium, potassium, silicon, strontium and zinc, all being present in bone and enamel and hence increasing biomimicry.[9]

FT-IR spectra (Fig. 3) indicate a very strong band at 1025 cm^{-1}, with a shoulder at 1092 (ν_3 antisymmetric PO stretching mode), and bands at 602 cm^{-1} and 560 cm^{-1} (ν_4 PO_4 antisymmetric bend), all compatible with natural fluorapatite.[73–75] The presence of carbonates is detected by the bands at 1450, 1419 (asymmetrical and symmetrical stretching modes of ν_3CO3) and 870 (ν_2CO_3, characteristic of beta-type substitution in HA[73–77]) cm^{-1}, indicating carbonate-substitution in fluorapatite. Finally, the organic phase (chitin) is revealed by the bands at 1640, 1538 and 1231 cm^{-1}, to be ascribed to amide II (N–H bending) and νC–O absorption, respectively.[78]

Table 1 EDS data for *L. anatina* seashell and the lingula-derived coatings

	F [wt%]	Ca/P at% ratio
Shell	0.06	1.75
Coating	6.33	1.60

SEM and EDS data (ESI,† Fig. S1 and S2), show that the outer surface of the shell is composed by a uniform fluorapatite layer.

For both strains, the MIC of the *L. anatina* seashell is lower compared to the MIC of the fluorapatite. In particular, the *L. anatina* MIC against *E. coli* is 80 mg mL^{-1} and three times lower than fluorapatite, whereas the MIC against *S. aureus* is 20 mg mL^{-1} and two times lower than fluorapatite ref. 79 and 80. These results indicate higher antibacterial efficacy compared to the synthetic analog not including the organic part. The increased antibacterial activity of the *L. anatina* seashell is likely due to the combination of the two antibacterial ions composing the inorganic part (about 68% in weight), mainly fluorine and zinc, together with the organic part composed of chitin/chitosan (about 32% in weight).

To study the antibacterial effect of the mineral part (*i.e.* the one that can be deposited in coating) and the effect of the organic part, we deproteinized the shell by heating it at 400 °C (ESI,† Fig. S4 and Table S1). Indeed, past results on *Discinisca tenuis* that has the same inorganic and organic composition as lingula, but a different structural organization, indicate that no

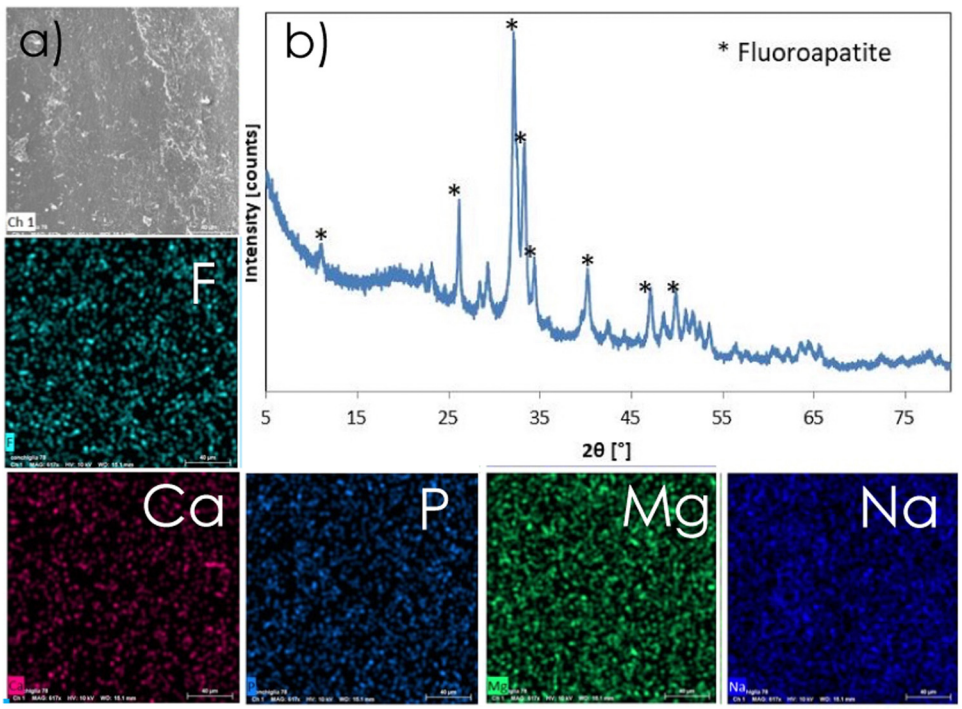

Fig. 2 (a) EDS and (b) XRD performed on *L. anatina* seashell.

Table 2 *L. anatina* seashell and coating composition, as assessed by ICP-MS

	Ca	K	Mg	Mn	Na	P	Si	Sr	Zn
	ppm	ppm	ppm	ppm	ppm	ppm	ppm	ppm	ppm
	Average ± st dev								
Shell	1299.00 ± 0.04	70.40 ± 2.65	95.11 ± 0.01	0.31 ± 0.01	246.00 ± 0.03	704.00 ± 0.00	133.40 ± 0.17	3.307 ± 0.00	0.98 ± 0.01
Coating	4.48 ± 0.29	0.13 ± 0.01	0.15 ± 0.00	0.01 ± 0.00	0.19 ± 0.02	1.40 ± 0.08	0.01 ± 0.00	0.03 ± 0.00	0.165 ± 0.01

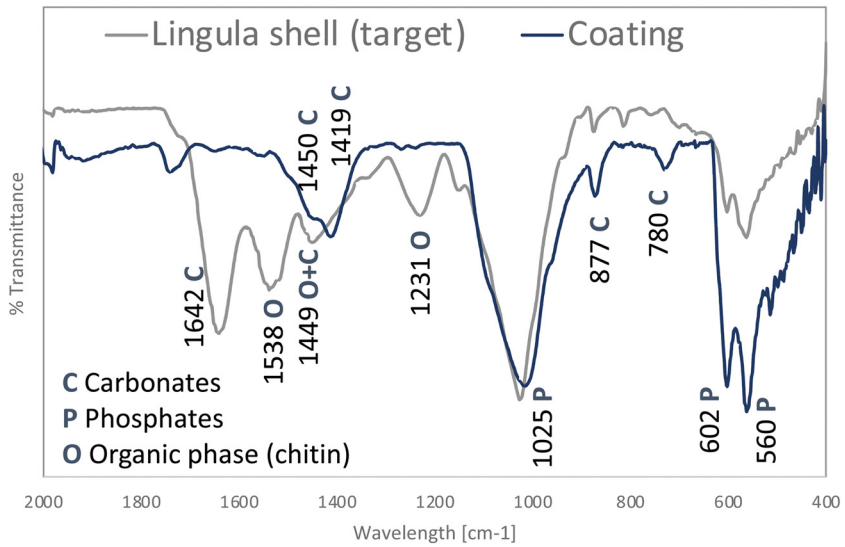

Fig. 3 FT-IR of *L. anatina* seashell before and after deposition in the form of nanostructured coatings.

modifications occurred at temperatures <700 °C, except for the decomposition of the organic part.[81] In our work, the results show that while the efficacy against *S. aureus* is not significantly modified after removing the organic part (99.37% CFU reduction), the antibacterial efficacy against *E. coli* drops significantly (84.15% CFU reduction, Fig. S4 and Table S1, ESI†). This result can be related with the mechanism of action of chitin/chitosan that seems to be active against the negatively charged lipopolysaccharides (LPS) and proteins located on the bacterial cell surface leading to the disruption of the cell envelope structure.[82] Therefore, the chitin/chitosan part of the *L. anatina* seashell significantly contributes to the antibacterial activity exerted against *E. coli* that is a Gram negative strain having an outer membrane with LPS molecules.[83] Further, *E. coli* was more susceptible to fluorapatite as compared to *L. anatina* seashell (MIC of fluorapatite is higher than *L. anatina* seashell in Table 3), indicating that the organic part of the shell (composed by chitin/chitosan) greatly contributes to the antibacterial effect against Gram negative strains. On the other hand, the activity against *S. aureus* is not significantly modified by the absence of chitosan suggesting that the inorganic part of the *L. anatina* seashell (fluorine and zinc) plays a critical role in the antibacterial activity towards this Gram positive strain. This is in line with previous studies revealing a significant inhibition exerted by zinc-based nanocoatings against *S. aureus* under both planktonic and biofilm growth conditions.[84] The antibacterial activity of these coatings is stronger against *S. aureus* compared to *E. coli*, probably due to an improved binding of zinc onto *S. aureus* cell surface or other events related with zinc cellular intake and interference with cellular mechanisms causing damage events including cell wall disruption, reactive oxygen species (ROS) production, and ATP synthesis inhibition.[62,84–86]

Table 3 Minimal inhibitory concentration of *L. anatina* seashell compared to fluorapatite against the growth of *Escherichia coli* and *Staphylococcus aureus* strains

	Fluorapatite (mg mL^{-1})	*L. anatina* seashell (mg mL^{-1})
Escherichia coli	240	80
Staphylococcus aureus	40	20

3.2. Nanostructured coatings deposition and characterization

Ionized jet deposition (IJT) was used to obtain nanostructured coatings of fluorapatite from the *L. anatina* seashell on a silica wafer substrate. The obtained coating was composed of aggregates with sizes ranging from 100 nm up to 1 μm, in many cases made of particles 20 nm in diameter (Fig. 4), characteristic of the deposition of CaP-based and ceramic-like materials by IJD. The surface of samples was homogeneous and no defects were noticed in any part of the samples.

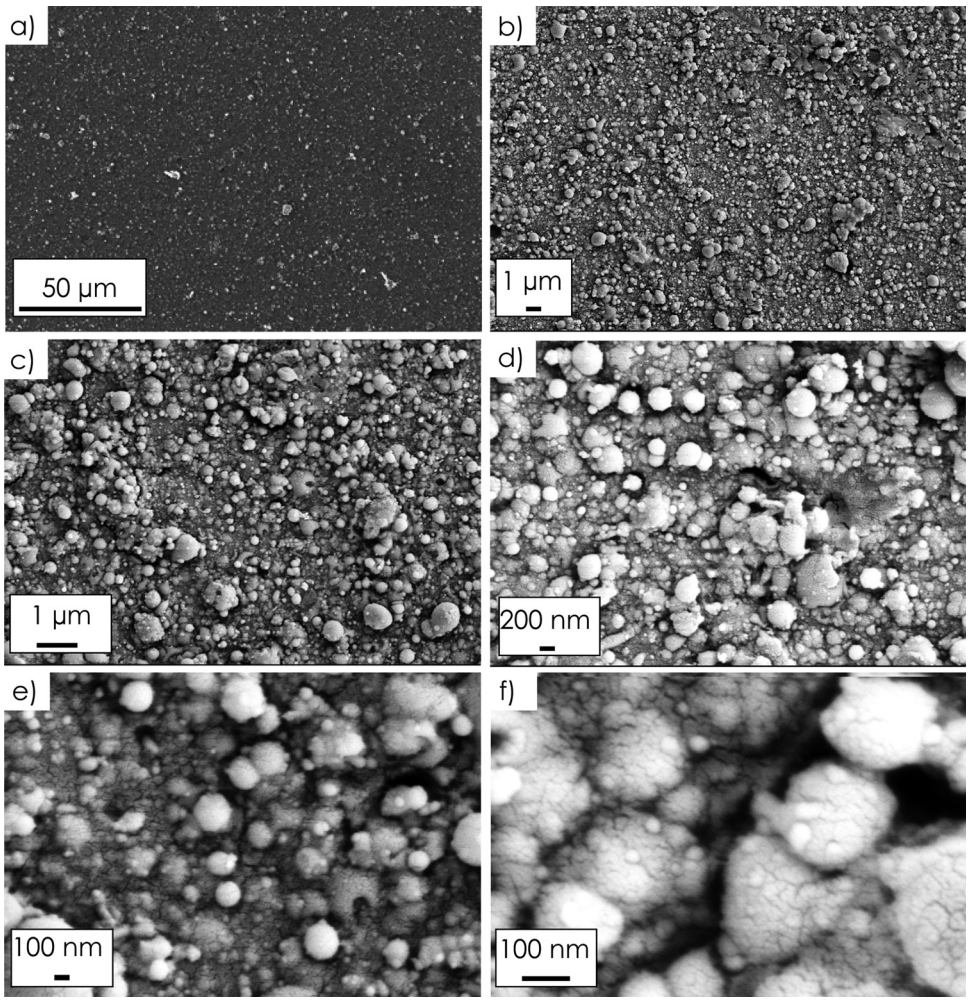

Fig. 4 Morphology of the nanostructured films obtained by IJD deposition of *L. anatina* seashell. Increasing magnification is shown from (a) to (f).

In FT-IR spectra (Fig. 3), bands observed for the coatings are the same as for the mineral part of *L. anatina* and are compatible with fluorapatite and carbonated hydroxyapatite. In our case, a distinction between fluorapatite and hydroxyapatite by FT-IR is not possible, due to the low crystallinity of the coatings, making FT-IR bands broad and ill-defined, while bands characteristic of carbonate substitutions can be clearly identified. The bands corresponding to the organic components are absent, showing their degradation during the IJD process. No other bands are assessed, so no metastable or decomposition phases are present in the film, as reported for similar techniques.

Regardless of the sample position and the incident angles the 2D-GIWAXS images show no diffraction signals but only diffused rings, typical of amorphous materials (Fig. 5(a)). The

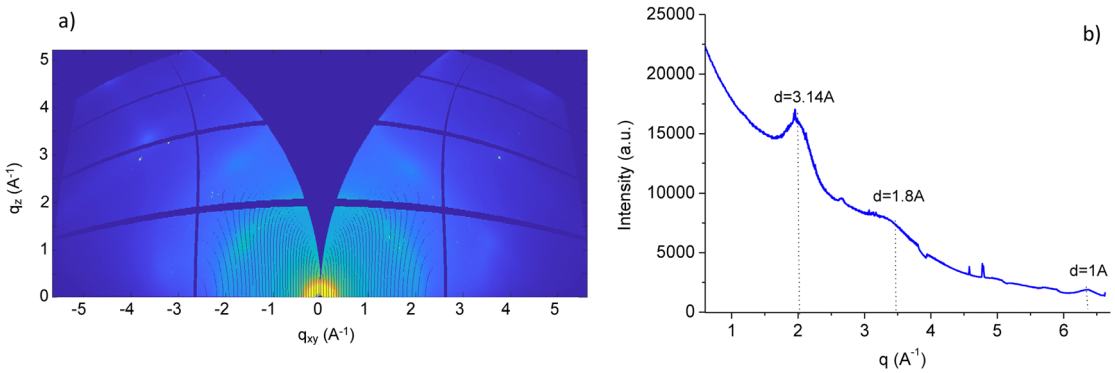

Fig. 5 (a) 2D-GIWAXS image of coated film recorded by using incident angle = 0.1°, (b) corresponding integrated intensity diffraction profile.

diffraction patterns obtained by integrating the intensity all over the image, indicate broad large peaks corresponding to periodicities of 1 Å, 1.8 Å and 3.14 Å (Fig. 5(b)).

This indicates that samples obtained by IJD are highly amorphous, consistently with what observed for biogenic hydroxyapatite.[61]

EDS data show that the Ca/P ratio is similar to that of the target material. In addition, fluorine is transferred in the coating, in a percentage higher than that of the target, indicating a preferential sputtering of fluorine (Table 1). ICP-MS data show that all trace elements present in the coating, including antibacterial zinc, are preserved in the coating, making it fully biomimetic (Table 2), although some preferential sputtering is observed. Indeed, starting from data of ICP-MS, we calculated the ratio between each substituent and calcium (Table S2, ESI†). Data indicate that all elements are transferred from the target to the coating, with K, Mg and Na being present in a similar, though lower concentration in the coating compared to the target, while Mn, Sr and, mostly, zinc, showing a preferential sputtering compared to calcium.

Altogether, however, our data show an excellent transfer in the composition between the target material and the coating with both the main mineral phase and all dopants present in the shell preserved in the coating.

Interestingly, from the point of view of IJD performance, if the seashell is not appropriately washed, also the NaCl crystals present in the seashell are decomposed and reconstructed in the coating, without changes of phase (Fig. S5, ESI†). This, of course, is detrimental for application in biomaterials, but is very important in terms of deposition performance, as it demonstrates the possibility to keep different phases in the target to be separated also in the coating, even when both phases are complex (here, a multi-doped hydroxyapatite and sodium chloride are present), have high tendency to

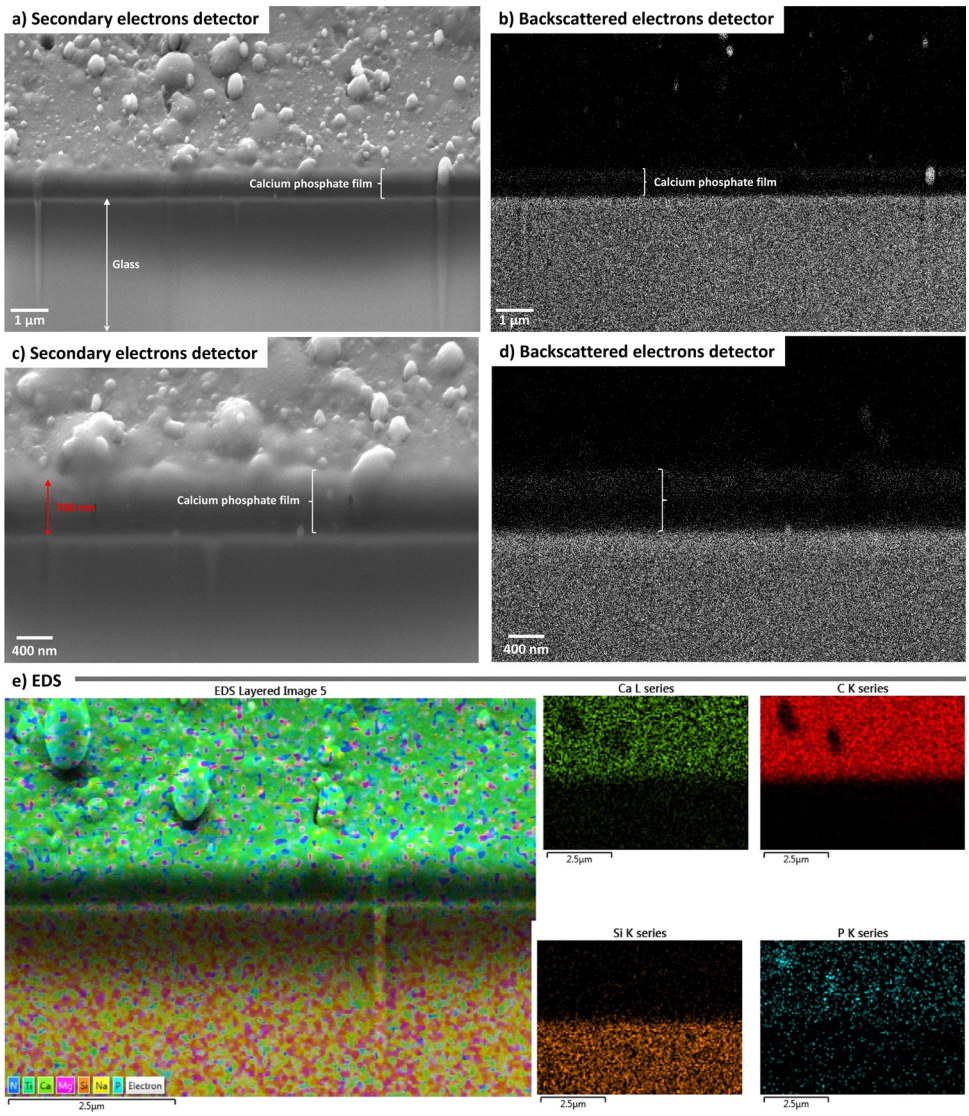

Fig. 6 FIB analyses of lingula films on glass substrates: imaging by secondary electron detector at lower (a) and higher (c) magnification; backscattered electrons imaging at (b) lower and (d) higher magnification; (e) EDS maps.

incorporate foreign ions (apatite) and/or when the two phases share the same ions (sodium).

3.3. Substrate influence on coatings characteristics

To study the properties of the coatings depending on the substrate and their applicability to different materials, we carried out a Focused Ion Beam-Scanning Electron Microscopy (FIB-SEM, Fig. 6–8) study comparing deposition on titanium alloy disks and on silicon wafers as reference materials. We then assessed the substrate influence on film thickness and microstructure.

Irrespective of the substrate, all films have a thickness of about 650 nm and a nanostructured surface morphology. However, significant modifications are observed when changing the substrate, as deposition onto polished titanium results in a rougher coating, characterized by the presence of coarser aggregates, while the films on glass and silicon are smoother.

When the coating was deposited onto glass and silicon, we observed the deposition of a homogeneous calcium phosphate film, with no evidence of porosity or defects. Some isolated coarser aggregates appeared on the surface.

While films on glass and silicon wafer were smooth (Fig. 6 and 7), the ones on Ti substrate were rough and non-uniform (Fig. 8). Although titanium disks were polished, we cannot exclude an influence of the substrate surface roughness on this parameter. As for the other coatings, no obvious internal structure or porosity is observed in the films.

These data indicate that some of the characteristics of the coatings, such as morphology, significantly depend on the substrate composition, suggesting that a specific optimization is needed for each substrate to be coated. On the other hand, other characteristics, such as thickness, are not influenced significantly by the substrate, while they strongly vary depending on the target.[87,88] Interestingly, the extent of this

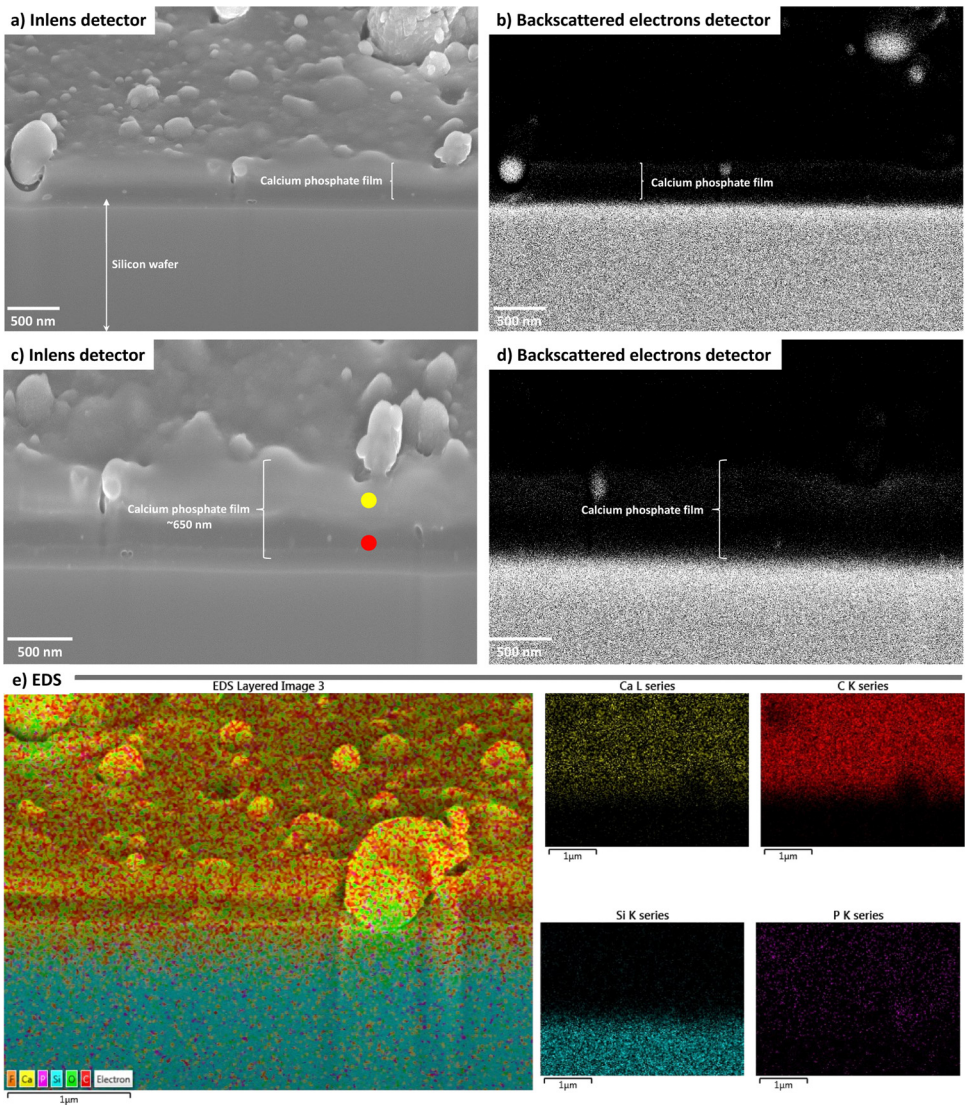

Fig. 7 FIB analyses of lingula films on silica wafers: (a) imaging by inlens detector at lower (a) and higher (c) magnification; backscattered electrons imaging at (b) lower and (d) higher magnification; (e) EDS maps.

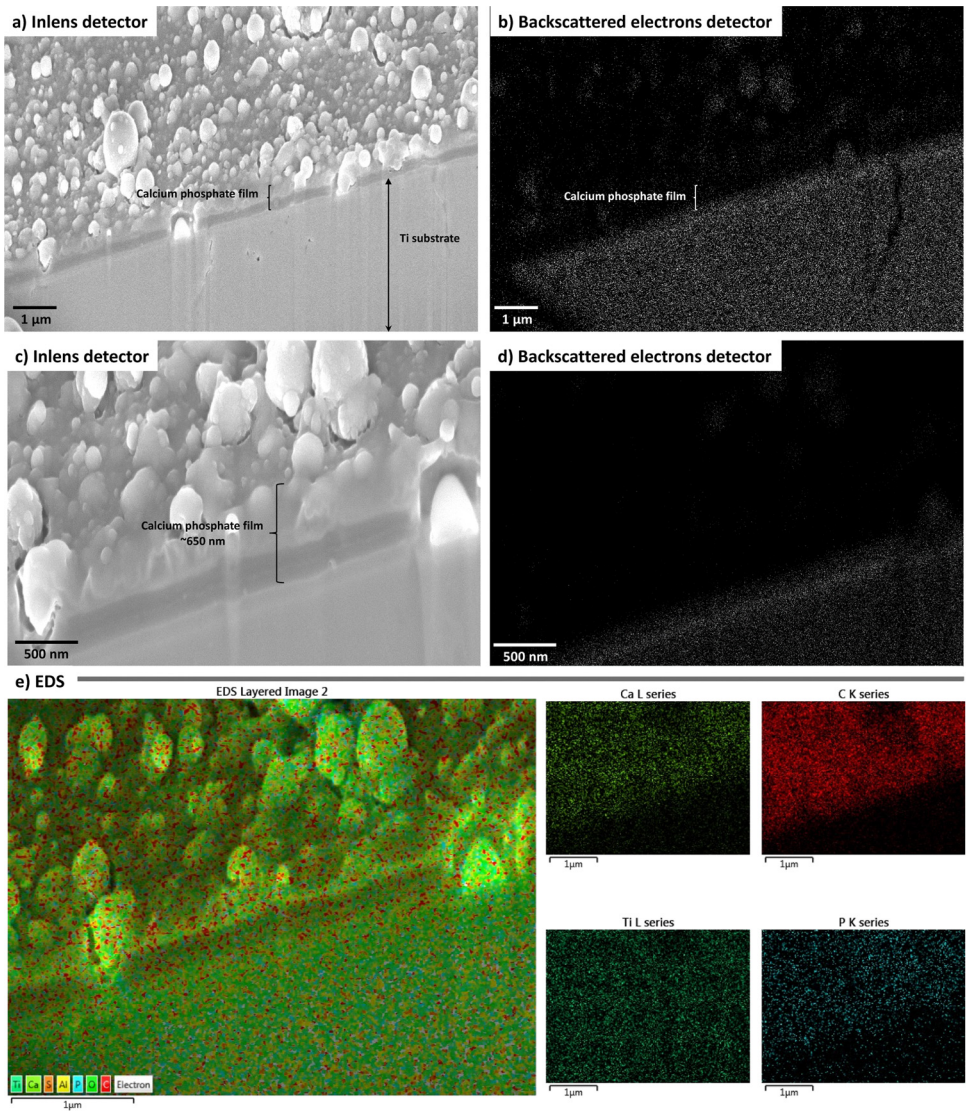

Fig. 8 FIB analyses of lingula films on microstructured titanium–aluminum–vanadium alloy substrates: (a) imaging by inlens detector at lower (a) and higher (c) magnification; backscattered electrons imaging at (b) lower and (d) higher magnification; (e) EDS maps.

dependence and the characteristics that are influenced is determined by the class of materials to which they are applied. Indeed, in the case of deposition onto polymers,[58,65] we observed that thickness significantly varies depending on the polymer surface charge, and so do coating composition, while surface morphology remains essentially unaltered.

3.4 *L. anatina* seashell coatings performance

Coatings are biocompatible, as reported in Fig. 9(a) where osteoblast-like cells MG-63 in direct contact with coating samples reported a good cell viability when compared to CTRL (no coating), with a notable cell proliferation over time and until 7 days of culture (Fig. 9(a)). When CM derived from coating was added to MG-63 cells, no cytotoxic effects due to the by-products are detected after 1 day of maintenance, except for a slight effect for the highest concentrated dilution (Fig. 9(b)).

Stability tests (Fig. 10) show that the coatings are stable in alpha-MEM medium until 21 days, so a prolonged antimicrobial effect is to be expected (data in progress). This is in contrast to coatings obtained by IJD of stoichiometric and ion-doped apatite in the absence of fluorine, which completely dissolve within 7 days.[61] We postulate that this enhanced stability of the coatings made from the *L. anatina* seashell derives from the fluorine content, which is known to reduce the solubility of apatite. The higher stability of these films can be especially promising for thermo-sensitive substrates, for which deposition in temperature is not permitted. When dissolution occurs, after 21 days, it happens without the formation of cracks or detachments, which would be detrimental, as they could cause inflammation and toxicity *in vivo*. In addition, dissolution of the coating is homogeneous, and we did not observe faster dissolution in specific areas of the coatings, which might suggest the presence of different phases in the

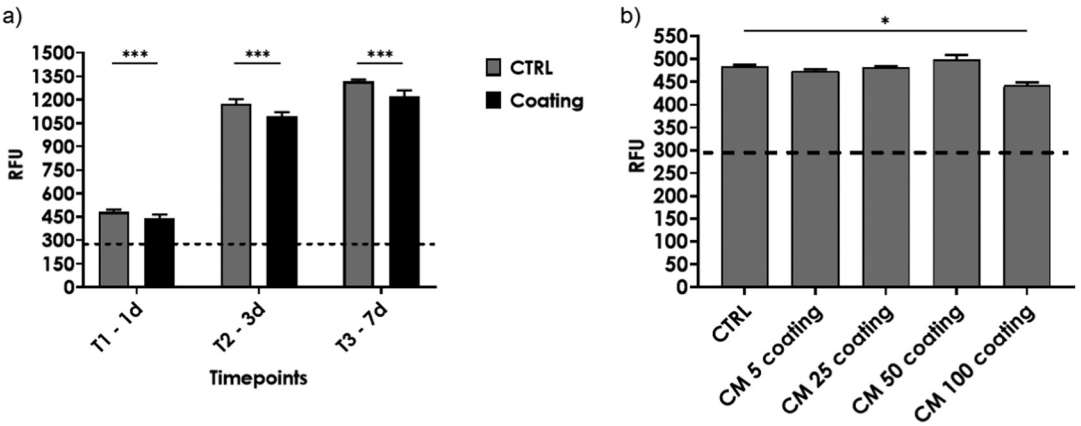

Fig. 9 (a) Cell viability of MG-63 with and without coating sample after 1 day (T1-1d), 3 days (T2-3d), and 7 days (T3-7d) of culture. (b) Cell viability of MG-63 after 24 h of maintenance with CM derived from coating at different dilutions with fresh culture medium (100 : 0, 50 : 50, 25 : 75, and 5 : 95). In both (a) and (b) panels, the dashed line is for CTRL at just seeded.

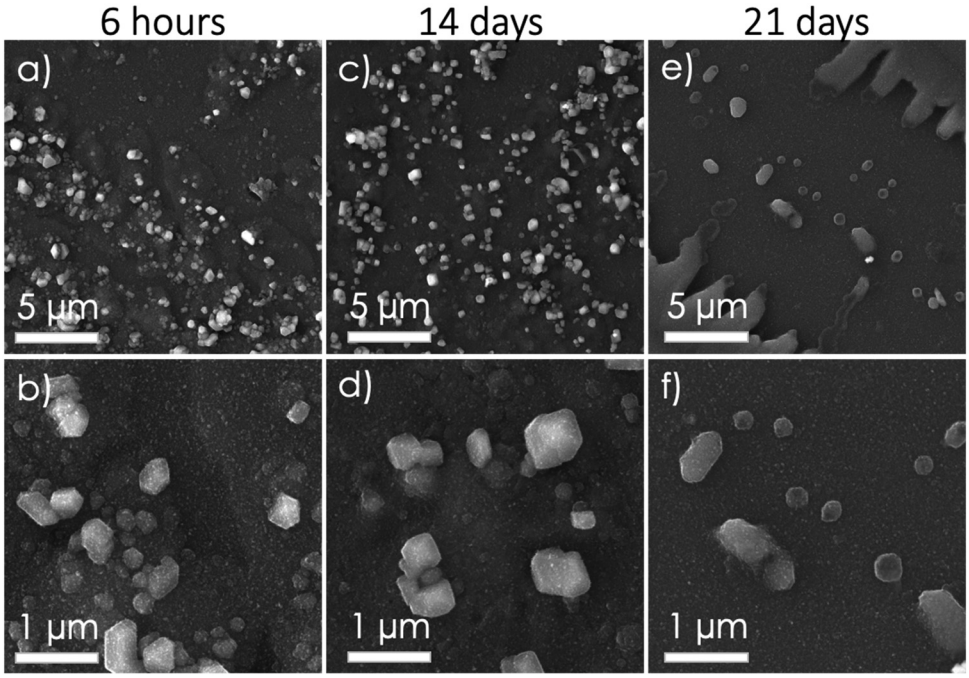

Fig. 10 Stability of *L. anatina* seashell coatings after immersion in medium for (a) and (b) 6 hours, (c) and (d), 14 days, (e) and (f) 21 days, as assessed by FEG-SEM.

coating. As a consequence, based on XRD, FT-IR and EDS data, we believe that the coating is composed by multi-substituted hydroxyapatite containing fluorine and carbonates (alongside the other mentioned ions) and not by a mix of fluorapatite and hydroxyapatite.

Coatings have antibacterial efficacy against both *E. coli* and *S. aureus* strains (Fig. S6, ESI†), with inhibition percentages of 88.83% and 99% of CFUs number compared to the control experiments, respectively. This correlates with the higher antibacterial efficacy of the seashell (fluorine and zinc-based), towards Gram-positive bacterial strains. On the other hand, the percentage of growth inhibition for the two bacteria is similar to that observed testing the deproteinized shell (Fig. S4, ESI†).

4. Conclusions

For the first time, we explore the possible use seashells and, in particular, of *L. anatina* seashell as a biomaterial for orthopedic and dental applications. Results obtained show that *L. anatina* seashell is composed by a carbonated fluorine-doped apatite, also containing traces of zinc, magnesium, strontium and

manganese. All these trace ions are contained in bone and dental enamel, thus making the coatings obtained from *L. anatina* biomimetic. Among the trace ions, fluorine and zinc also show potential antimicrobial activity. Furthermore, for the first time, we demonstrate that, thanks to the combination of this unique mineral phase and an organic part constituted by chitin, *L. anatina* seashell has high antibacterial activity against both Gram-positive and Gram-negative strains, thus resulting more antibacterial than synthetic fluorapatite, as denoted by the significantly lower Minimal Inhibitory Concentration (MIC) of *L. anatina* seashell compared to fluorapatite. The mineral part alone shows higher efficacy against the Gram positive *S. aureus* strain and a more moderate effect on the Gram negative *E. coli* strain.

Upon deposition by IJD, nanostructured biomimetic coatings can be obtained, having the same composition as the inorganic phase of *L. anatina* seashell. Indeed, we show that IJD permits a good conservation of the target stoichiometry, avoiding the formation of secondary products and/or a poor conservation of ion doping, which often occur with many plasma-assisted techniques.

The thickness of the coatings (650 nm) is independent of the substrate to which it is applied, while surface morphology strongly depends on the characteristics of the device. Coatings are biocompatible and stable for over 21 days of immersion in α-MEM medium. In addition, they cause a high reduction of viability on *S. aureus*, and a moderate effect on *E. coli*. The effect is dose-dependent, thus causing the delay/impairment of bacterial growth when supplied at low concentration and exerting a toxic/killing effect towards bacteria when added at high concentration.

Our results show that deposition from seashells is possible by IJD, and represent a promising route to obtain biomimetic biomaterials. In addition, thanks to its biomimicry and special properties, we believe lingula shell is a very promising material for orthopedics and dentistry, to produce nanostructured coatings and impart antibacterial functionalization to different devices.

Conflicts of interest

The authors declare no conflict of interest.

Acknowledgements

This work was supported by funding from the Royal Society of Edinburgh Saltire International Collaboration Award, grant no. 1887, to FN, GF and GG. NB acknowledges funding from 5 × 1000 Anno 2019, Redditi 2018 ''MEDICINA RIGENERATIVA E RIPARATIVA PERSONALIZZATA PER LE PATOLOGIE DEI TESSUTI MUSCOLO-SCHELETRICI E LA CHIRURGIA RICOSTRUTTIVA ORTOPEDICA''. FIB-SEM was performed at the facility at the University of Edinburgh (EPSRC grant no. EP/P030564/1). Dr Michele Iafisco (National Research Council, Istituto di Scienza, Tecnologia e Sostenibilità per lo Sviluppo dei Materiali Ceramici, ISSMC-CNR, Faenza, Italy) is kindly acknowledged for providing synthetic fluorapatite.

References

1 M. Šupová, Substituted hydroxyapatites for biomedical applications: A review, *Ceram. Int.*, 2015, **41**, 9203–9231.
2 S. V. Dorozhkin, Calcium orthophosphate coatings, films and layers, *Prog. Biomater.*, 2012, **1**, 1–40.
3 R. A. Surmenev, M. A. Surmeneva and A. A. Ivanova, Significance of calcium phosphate coatings for the enhancement of new bone osteogenesis – a review, *Acta Biomater.*, 2014, **10**, 557–579.
4 I. V. Antoniac, M. Filipescu, K. Barbaro, A. Bonciu, R. Birjega, C. M. Cotrut, E. Galvano, M. Fosca, I. V. Fadeeva, G. Vadalà, M. Dinescu and J. V. Rau, Iron Ion-Doped Tricalcium Phosphate Coatings Improve the Properties of Biodegradable Magnesium Alloys for Biomedical Implant Application, *Adv. Mater. Interfaces*, 2020, **7**, 2000531.
5 K. A. Prosolov, M. A. Khimich, J. V. Rau, D. V. Lychagin and Y. P. Sharkeev, Influence of oblique angle deposition on Cu-substituted hydroxyapatite nano-roughness and morphology, *Surf. Coat. Technol.*, 2020, **394**, 125883.
6 B. Istrate, J. V. Rau, C. Munteanu, I. V. Antoniac and V. Saceleanu, Properties and *in vitro* assessment of ZrO_2-based coatings obtained by atmospheric plasma jet spraying on biodegradable Mg–Ca and Mg–Ca–Zr alloys, *Ceram. Int.*, 2020, **46**, 15897–15906.
7 T. V. Safronova, I. I. Selezneva, S. A. Tikhonova, A. S. Kiselev, G. A. Davydova, T. B. Shatalova, D. S. Larionov and J. V. Rau, Biocompatibility of biphasic α,β-tricalcium phosphate ceramics *in vitro*, *Bioact. Mater.*, 2020, **5**, 423–427.
8 A. Bigi and E. Boanini, Functionalization of octacalcium phosphate for bone replacement, in *Octacalcium Phosphate Biomaterials*, ed. O. Suzuki and G. Insley, Woodhead Publishing, UK, 2020, pp. 37–54.
9 E. Boanini, M. Gazzano and A. Bigi, Ionic substitutions in calcium phosphates synthesized at low temperature, *Acta Biomater.*, 2010, **6**, 1882–1894.
10 F. Salamanna, G. Giavaresi, D. Contartese, A. Bigi, E. Boanini, A. Parrilli, R. Lolli, A. Gasbarrini, G. Barbanti Brodano and M. Fini, Effect of strontium substituted ß-TCP associated to mesenchymal stem cells from bone marrow and adipose tissue on spinal fusion in healthy and ovariectomized rat, *J. Cell. Physiol.*, 2019, **234**, 20046–20056.
11 W. R. Fordham, S. Redmond, A. Westerland, E. G. Cortes, C. Walker, C. Gallagher, C. J. Medina, F. Waecther, C. Lunk, R. F. Ostrum, G. A. Caputo, J. D. Hettinger and R. R. Krchnavek, Silver as a Bactericidal Coating for Biomedical Implants, *Surf. Coat. Technol.*, 2014, **253**, 52–57.
12 V. Alt, Antimicrobial coated implants in trauma and orthopedics-A clinical review and risk-benefit analysis, *Injury*, 2017, **48**, 599–607.
13 J. Raphel, M. Holodniy, S. B. Goodman and S. C. Heilshorn, Multifunctional coatings to simultaneously promote

osseointegration and prevent infection of orthopaedic implants, *Biomaterials*, 2016, **84**, 301–314.

14 T. M. Fernandes Patrício, D. Mumcuoglu, M. Montesi, S. Panseri, J. Witte-Bouma, S. F. Garcia, M. Sandri, A. Tampieri, E. Farrell and S. Sprio, Bio-inspired polymeric iron-doped hydroxyapatite microspheres as a tunable carrier of rhBMP-2, *Mater. Sci. Eng., C*, 2021, **119**, 111410.

15 M. B. Sedelnikova, E. G. Komarova, Y. P. Sharkeev, A. V. Ugodchikova, T. V. Tolkacheva, J. V. Rau, E. E. Buyko, V. V. Ivanov and V. V. Sheikin, Modification of titanium surface *via* Ag-, Sr- and Si-containing micro-arc calcium phosphate coating, *Bioact. Mater.*, 2019, **4**, 224–235.

16 K. A. Prosolov, O. A. Belyavskaya, J. Linders, K. Loza, O. Prymak, C. Mayer, J. V. Rau, M. Epple and Y. P. Sharkeev, Glancing Angle Deposition of Zn-Doped Calcium Phosphate Coatings by RF Magnetron Sputtering, *Coatings*, 2019, **9**, 220.

17 J. V. Rau, M. Curcio, M. G. Raucci, K. Barbaro, I. Fasolino, R. Teghil, L. Ambrosio, A. De Bonis and A. R. Boccaccini, Cu-Releasing Bioactive Glass Coatings and Their *in Vitro* Properties, *ACS Appl. Mater. Interfaces*, 2019, **11**, 5812–5820.

18 A. Ballardini, M. Montesi, S. Panseri, A. Vandini, P. G. Balboni, A. Tampieri and S. Sprio, New hydroxyapatite nanophases with enhanced osteogenic and anti-bacterial activity, *J. Biomed. Mater. Res., Part A*, 2018, **106**, 521–530.

19 L. Forte, S. Sarda, P. Torricelli, C. Combes, F. Brouillet, O. Marsan, F. Salamanna, M. Fini, E. Boanini and A. Bigi, Multifunctionalization Modulates Hydroxyapatite Surface Interaction with Bisphosphonate: Antiosteoporotic and Antioxidative Stress Materials, *ACS Biomater. Sci. Eng.*, 2019, **5**, 3429–3439.

20 G. Graziani, M. Boi and M. Bianchi, A Review on Ionic Substitutions in Hydroxyapatite Thin Films: Towards Complete Biomimetism, *Coatings*, 2018, **8**, 269.

21 G. Graziani, M. Bianchi, E. Sassoni, A. Russo and M. Marcacci, Ion-substituted calcium phosphate coatings deposited by plasma-assisted techniques: A review, *Mater. Sci. Eng., C*, 2017, **74**, 219–229.

22 S. Sprio, M. Dapporto, L. Preti, E. Mazzoni, M. R. Iaquinta, F. Martini, M. Tognon, N. M. Pugno, E. Restivo, L. Visai and A. Tampieri, Enhancement of the biological and mechanical performances of sintered hydroxyapatite by multiple ions doping, *Front. Mater.*, 2020, **7**, 224.

23 A. De Bonis, V. Uskoković, K. Barbaro, I. Fadeeva, M. Curcio, L. Imperatori, R. Teghil and J. V. Rau, Pulsed laser deposition temperature effects on strontium-substituted hydroxyapatite thin films for biomedical implants, *Cell Biol. Toxicol.*, 2020, **36**, 537–551.

24 I. V. Fadeeva, V. I. Kalita, D. I. Komlev, A. A. Radiuk, A. S. Fomin, G. A. Davidova, N. K. Fursova, F. F. Murzakhanov, M. R. Gafurov, M. Fosca, I. V. Antoniac, S. M. Barinov and J. V. Rau, *In Vitro* Properties of Manganese-Substituted Tricalcium Phosphate Coatings for Titanium Biomedical Implants Deposited by Arc Plasma, *Materials*, 2020, **13**, 4411.

25 C. Capuccini, P. Torricelli, F. Sima, E. Boanini, C. Ristoscu, B. Bracci, G. Socol, M. Fini, I. N. Mihailescu and A. Bigi, Strontium-substituted hydroxyapatite coatings synthesized by pulsed-laser deposition: *in vitro* osteoblast and osteoclast response, *Acta Biomater.*, 2008, **4**, 1885–1893.

26 H. Madupalli, B. Pavan and M. M. J. Tecklenburg, Carbonate substitution in the mineral component of bone: Discriminating the structural changes, simultaneously imposed by carbonate in A and B sites of apatite, *J. Solid State Chem.*, 2017, **255**, 27–35.

27 J. V. Rau, A. Generosi, S. Laureti, V. S. Komlev, D. Ferro, S. N. Cesaro, B. Paci, V. R. Albertini, E. Agostinelli and S. M. Barinov, Physicochemical investigation of pulsed laser deposited carbonated hydroxyapatite films on titanium, *ACS Appl. Mater. Interfaces*, 2009, **1**, 1813–1820.

28 G. Borciani, T. Fischetti, G. Ciapetti, M. Montesissa, N. Baldini and G. Graziani, Marine biological waste as a source of hydroxyapatite for bone tissue engineering applications, *Ceram. Int.*, 2023, **49**, 1572–1584.

29 W. Mróz, A. Bombalska, S. Burdyńska, M. Jedyński, A. Prokopiuk, B. Budner, A. Ślósarczyk, A. Zima, E. Menaszek, A. Ścisłowska-Czarnecka and K. Niedzielski, Structural studies of magnesium doped hydroxyapatite coatings after osteoblast culture, *J. Mol. Struct.*, 2010, **977**, 145–152.

30 E. S. Bogya, Z. Károly and R. Barabás, Atmospheric plasma sprayed silica–hydroxyapatite coatings on magnesium alloy substrates, *Ceram. Int.*, 2015, **41**, 6005–6012.

31 W. Mróz, M. Jedyński, A. Prokopiuk, A. Ślósarczyk and Z. Paszkiewicz, Characterization of calcium phosphate coatings doped with Mg, deposited by pulsed laser deposition technique using ArF excimer laser, *Micron*, 2009, **40**, 140–142.

32 W. Mróz, B. Budner, R. Syroka, K. Niedzielski, G. Golański, A. Slósarczyk, D. Schwarze and T. E. Douglas, In vivo implantation of porous titanium alloy implants coated with magnesium-doped octacalcium phosphate and hydroxyapatite thin films using pulsed laser deposition, *J. Biomed. Mater. Res., Part B*, 2015, **103**, 151–158.

33 M. A. Surmeneva, M. V. Chaikina, V. I. Zaikovskiy, V. F. Pichugin, V. Buck, O. Prymak, M. Epple and R. A. Surmenev, The structure of an RF-magnetron sputter-deposited silicate-containing hydroxyapatite-based coating investigated by high-resolution techniques, *Surf. Coat. Technol.*, 2013, **218**, 39–46.

34 M. A. Surmeneva, T. M. Mukhametkaliyev, A. I. Tyurin, A. D. Teresov, N. N. Koval, T. S. Pirozhkova, I. A. Shuvarin, A. V. Shuklinov, A. O. Zhigachev, C. Oehr and R. A. Surmenev, Effect of silicate doping on the structure and mechanical properties of thin nanostructured RF magnetron sputter-deposited hydroxyapatite films, *Surf. Coat. Technol.*, 2015, **275**, 176–184.

35 M. A. Surmeneva, R. A. Surmenev, V. F. Pichugin, S. S. Chernousova and M. Epple, In-vitro investigation of magnetron-sputtered coatings based on silicon-substituted hydroxyapatite, *J. Surf. Invest.*, 2011, **5**, 1202–1207.

36 V. F. Pichugin, M. A. Surmeneva, R. A. Surmenev, I. A. Khlusov and M. Epple, Study of physicochemical and biological properties of calcium phosphate coatings

prepared by RF magnetron sputtering of silicon-substituted hydroxyapatite, *J. Surf. Invest.*, 2011, **5**, 863–869.

37 M. Surmeneva, A. Tyurin, T. Mukhametkaliyev, A. Teresov, A. Koval, T. Pirozhkova, I. Shuvarin, E. Chudinova and R. Surmenev, The effect of Si content on structure and mechanical features of silicon-containing calcium-phosphate-based films deposited by RF-magnetron sputtering on titanium substrate treated by pulsed electron beam, *IOP Conf. Ser.: Mater. Sci. Eng.*, 2015, **98**, 012028.

38 E. S. Thian, J. Huang, S. M. Best, Z. H. Barber and W. Bonfield, Silicon-substituted hydroxyapatite: The next generation of bioactive coatings, *Mater. Sci. Eng., C*, 2007, **27**, 251–256.

39 J. V. Rau, M. Fosca, I. Cacciotti, S. Laureti, A. Bianco and R. Teghil, Nanostructured Si-substituted hydroxyapatite coatings for biomedical applications, *Thin Solid Films*, 2013, **543**, 167–170.

40 J. V. Rau, I. Cacciotti, S. Laureti, M. Fosca, G. Varvaro and A. Latini, Bioactive, nanostructured Si-substituted hydroxyapatite coatings on titanium prepared by pulsed laser deposition, *J. Biomed. Mater. Res., Part B*, 2015, **103**, 1621–1631.

41 E. György, P. Toricelli, G. Socol, M. Iliescu, I. Mayer, I. N. Mihailescu, A. Bigi and J. Werckman, Biocompatible Mn^{2+}-doped carbonated hydroxyapatite thin films grown by pulsed laser deposition, *J. Biomed. Mater. Res., Part A*, 2004, **71**, 353–358.

42 M. Iafisco, L. Degli Esposti, G. B. Ramírez-Rodríguez, F. Carella, J. Gómez-Morales, A. C. Ionescu, E. Brambilla, A. Tampieri and J. M. Delgado-López, Fluoride-doped amorphous calcium phosphate nanoparticles as a promising biomimetic material for dental remineralization, *Sci. Rep.*, 2018, **8**, 17016.

43 E. O. López, A. L. Rossi, B. S. Archanjo, R. O. Ospina, A. Mello and A. M. Rossi, Crystalline nano-coatings of fluorine-substituted hydroxyapatite produced by magnetron sputtering with high plasma confinement, *Surf. Coat. Technol.*, 2015, **264**, 163–174.

44 L. Borkowski, A. Przekora, A. Belcarz, K. Palka, G. Jozefaciuk, T. Lübek, M. Jojczuk, A. Nogalski and G. Ginalska, Fluorapatite ceramics for bone tissue regeneration: Synthesis, characterization and assessment of biomedical potential, *Mater. Sci. Eng., C*, 2020, **116**, 111211.

45 E. Cianflone, F. Brouillet, D. Grossin, J. Soulié, C. Josse, S. Vig, M. H. Fernandes, C. Tenailleau, B. Duployer, C. Thouron and C. Drouet, Toward Smart Biomimetic Apatite-Based Bone Scaffolds with Spatially Controlled Ion Substitutions, *Nanomaterials*, 2023, **13**, 519.

46 A. De Bonis, V. Uskoković, K. Barbaro, I. Fadeeva, M. Curcio, L. Imperatori, R. Teghil and J. V. Rau, Pulsed laser deposition temperature effects on strontium-substituted hydroxyapatite thin films for biomedical implants, *Cell Biol. Toxicol.*, 2020, **36**, 537–551.

47 A. Ruffini, M. Sandri, M. Dapporto, E. Campodoni, A. Tampieri and S. Sprio, Nature-Inspired Unconventional Approaches to Develop 3D Bioceramic Scaffolds with Enhanced Regenerative Ability, *Biomedicines*, 2021, **9**, 916.

48 M. Vukomanovic, L. Gazvoda, N. Anicic, M. Rubert, D. Suvorov, R. Müller and S. Hofmann, Multi-doped apatite: Strontium, magnesium, gallium and zinc ions synergistically affect osteogenic stimulation in human mesenchymal cells important for bone tissue engineering, *Biomater. Adv.*, 2022, **140**, 213051.

49 J. V. Rau, I. Cacciotti, A. De Bonis, M. Fosca, V. S. Komlev, A. Latini, A. Santagata and R. Teghil, Fe-doped hydroxyapatite coatings for orthopedic and dental implant applications, *Appl. Surf. Sci.*, 2014, **307**, 301–305.

50 N. Gugala, J. A. Lemire and R. J. Turner, The efficacy of different anti-microbial metals at preventing the formation of, and eradicating bacterial biofilms of pathogenic indicator strains, *J. Antibiot.*, 2017, **70**, 775–780.

51 L. Duta, N. Mihailescu, A. C. Popescu, C. R. Luculescu, I. N. Mihailescu, G. Çetin, O. Gunduz, F. N. Oktar, A. C. Popa, A. Kuncser, C. Besleaga and G. E. Stan, Comparative physical, chemical and biological assessment of simple and titanium-doped ovine dentine-derived hydroxyapatite coatings fabricated by pulsed laser deposition, *Appl. Surf. Sci.*, 2017, **413**, 129–139.

52 L. Duta, F. N. Oktar, G. E. Stan, G. Popescu-Pelin, N. Serban, C. Luculescu and I. N. Mihailescu, Novel doped hydroxyapatite thin films obtained by pulsed laser deposition, *Appl. Surf. Sci.*, 2013, **265**, 41–49.

53 S. Scialla, F. Carella, M. Dapporto, S. Sprio, A. Piancastelli, B. Palazzo, A. Adamiano, L. Degli Esposti, M. Iafisco and C. Piccirillo, Mussel Shell-Derived Macroporous 3D Scaffold: Characterization and Optimization Study of a Bioceramic from the Circular Economy, *Mar. Drugs*, 2020, **18**, 309.

54 D. Bigoni, R. Cavuoto, D. Misseroni, M. Paggi, A. Ruffini, S. Sprio and A. Tampieri, Ceramics with the signature of wood: a mechanical insight, *Mater. Today Bio*, 2019, **5**, 100032.

55 N. Mihailescu, G. E. Stan, L. Duta, M. C. Chifiriuc, C. Bleotu, M. Sopronyi, C. Luculescu, F. N. Oktar and I. N. Mihailescu, Structural, compositional, mechanical characterization and biological assessment of bovine-derived hydroxyapatite coatings reinforced with MgF_2 or MgO for implants functionalization, *Mater. Sci. Eng., C*, 2016, **59**, 863–874.

56 G. Popescu-Pelin, C. Ristoscu, L. Duta, G. E. Stan, I. Pasuk, T. Tite, M. S. Stan, C. Bletou, M. Popa, M. C. Chifiriuc, F. N. Oktar, A. Nicarel and I. N. Mihailescu, Antimicrobial and cytocompatible bovine hydroxyapatite-alumina-zeolite composite coatings synthesized by pulsed laser deposition from low-cost sustainable natural resources, *ACS Sustainable Chem. Eng.*, 2020, **8**, 4026–4036.

57 D. Chioibasu, L. Duta, G. Popescu-Pelin, N. Popa, N. Milodin, S. Iosub, L. M. Balescu, A. Catalin Galca, A. Claudiu Popa, F. N. Oktar, G. E. Stan and A. C. Popescu, Animal Origin Bioactive Hydroxyapatite Thin Films Synthesized by RF-Magnetron Sputtering on 3D Printed Cranial Implants, *Metals*, 2019, **9**, 1332.

58 G. Di Pompo, A. Liguori, M. Carlini, S. Avnet, M. Boi, N. Baldini, M. L. Focarete, M. Bianchi, C. Gualandi and G. Graziani, Electrospun fibers coated with nanostructured

biomimetic hydroxyapatite: A new platform for regeneration at the bone interfaces, *Biomater. Adv.*, 2023, **144**, 213231.

59 M. Sartori, G. Graziani, E. Sassoni, S. Pagani, M. Boi, M. C. Maltarello, N. Baldini and M. Fini, Nanostructure and biomimetics orchestrate mesenchymal stromal cell differentiation: An *in vitro* bioactivity study on new coatings for orthopedic applications, *Mater. Sci. Eng., C*, 2021, **123**, 112031.

60 G. Graziani, M. Govoni, L. Vivarelli, M. Boi, M. De Carolis, M. Bianchi, E. Sassoni, M. C. Bignozzi, G. Carnevale, F. Marmi, M. C. Maltarello and D. Dallari, A Comprehensive Microstructural and Compositional Characterization of Allogenic and Xenogenic Bone: Application to Bone Grafts and Nanostructured Biomimetic Coatings, *Coatings*, 2020, **10**, 522.

61 G. Graziani, M. Berni, A. Gambardella, M. De Carolis, M. C. Maltarello, M. Boi, G. Carnevale and M. Bianchi, Fabrication and characterization of biomimetic hydroxyapatite thin films for bone implants by direct ablation of a biogenic source, *Mater. Sci. Eng., C*, 2019, **99**, 853–862.

62 D. Ghezzi, M. Boi, E. Sassoni, F. Valle, E. Giusto, E. Boanini, N. Baldini, M. Cappelletti and G. Graziani, Customized biofilm device for antibiofilm and antibacterial screening of newly developed nanostructured silver and zinc coatings, *J. Biol. Eng.*, 2023, **17**, 18.

63 D. Ghezzi, E. Sassoni, M. Boi, M. Montesissa, N. Baldini, G. Graziani and M. Cappelletti, Antibacterial and Antibiofilm Activity of Nanostructured Copper Films Prepared by Ionized Jet Deposition, *Antibiotics*, 2022, **12**, 55.

64 G. Graziani, K. Barbaro, I. V. Fadeeva, D. Ghezzi, M. Fosca, E. Sassoni, G. Vadalà, M. Cappelletti, F. Valle, N. Baldini and J. V. Rau, Ionized jet deposition of antimicrobial and stem cell friendly silver-substituted tricalcium phosphate nanocoatings on titanium alloy, *Bioact. Mater.*, 2021, **6**, 2629–2642.

65 G. Pagnotta, G. Graziani, N. Baldini, A. Maso, M. L. Focarete, M. Berni, F. Biscarini, M. Bianchi and C. Gualandi, Nanodecoration of electrospun polymeric fibers with nanostructured silver coatings by ionized jet deposition for antibacterial tissues, *Mater. Sci. Eng., C*, 2020, **113**, 110998.

66 A. Maidaniuc, F. Miculescu, R. Cătălin Ciocoiu, T. Mihai Butte, I. Pasuk, G. E. Stan, S. I. Voicu and L. Toma Ciocan, Effect of the processing parameters on surface, physicochemical and mechanical features of bioceramics synthesized from abundant carp fish bones, *Ceram. Int.*, 2020, **46**, 10159–10171.

67 A. Williams, M. Cusack and J. O. Buckman, Chemicostructural phylogeny of the discinoid brachiopod shell, *Philos. Trans. R. Soc., B*, 1998, **353**, 2005–2038.

68 R. Z. LeGeros, C. M. Pan, S. Suga and N. Watabe, Crystallochemical properties of apatite in atremate brachiopod shells, *Calcif. Tissue Int.*, 1985, **37**, 98–100.

69 O. B. A. Agbaje, G. A. Brock, Z. Zhang, K. C. Duru, Y. Liang, S. C. George and L. E. Holmer, Biomacromolecules in recent phosphate-shelled brachiopods: identification and characterization of chitin matrix, *J. Mater. Sci.*, 2021, **56**, 19884–19898.

70 A. Williams and M. Cusack, Evolution of a rhythmic lamination in the organophosphatic shells of brachiopods, *J. Struct. Biol.*, 1999, **126**, 227–240.

71 L. Leroux and J. L. Lacout, Synthesis of calcium-strontium phosphate fluor-hydroxyapatites by neutralization, *Phosphorus, Sulfur Silicon Relat. Elem.*, 2001, **173**(1), 27–38.

72 P. Ptáček, Identification, Characterization and Properties of Apatites, in *Apatites and their Synthetic Analogues – Synthesis, Structure, Properties and Applications*, ed. P. Ptáček, InTechOpen, London, 2016.

73 I. Rehman and W. Bonfield, Characterization of hydroxyapatite and carbonated apatite by photo acoustic FTIR spectroscopy, *J. Mater. Sci. Mater. Med*, 1997, **8**, 1–4.

74 A. Antonakos, E. Liarokapis and T. Leventouri, Micro-Raman and FTIR studies of synthetic and natural apatites, *Biomaterials*, 2007, **28**, 3043–3054.

75 V. Vandeginste, C. Cowan, R. L. Gomes, T. Hassan and J. Titman, Natural fluorapatite dissolution kinetics and Mn^{2+} and Cr^{3+} metal removal from sulfate fluids at 35 °C, *J. Hazard. Mater.*, 2020, **389**, 122150.

76 M. E. Fleet, Infrared spectra of carbonate apatites: ν_2-Region bands, *Biomaterials*, 2009, **30**, 1473–1481.

77 K. Prabu and E. Natarajan, Isolation and FTIR spectroscopy characterization of chitin from local sources, *Adv. Appl. Sci. Res.*, 2012, **3**, 1870–1875.

78 E. M. Dahmane, M. Taourirte, N. Eladlani and M. Rhazi, Extraction and characterization of chitin and chitosan from Parapenaeus longirostris from Moroccan local sources, *Int. J. Polym. Anal. Charact.*, 2014, **19**, 342–351.

79 R. E. Marquis, Antimicrobial actions of fluoride for oral bacteria, *Can. J. Microbiol.*, 1995, **41**, 955–964.

80 A. Alhilou, T. Do, L. Mizban, B. H. Clarkson, D. J. Wood and M. G. Katsikogianni, Physicochemical and Antibacterial Characterization of a Novel Fluorapatite Coating, *ACS Omega*, 2016, **1**, 264–276.

81 J. Ihli, A. S. Schenk and S. Rosenfeldt, *et al.*, Mechanical adaptation of brachiopod shells *via* hydration-induced structural changes, *Nat. Commun.*, 2021, **12**, 5383.

82 H. Yilmaz Atay, Antibacterial Activity of Chitosan-Based Systems, *Functional Chitosan*, 2020, **6**, 457–489.

83 I. M. Helander, E. L. Nurmiaho-Lassila, R. Ahvenainen, J. Rhoades and S. Roller, Chitosan disrupts the barrier properties of the outer membrane of Gram-negative bacteria, *Int. J. Food Microbiol.*, 2001, **71**, 235–244.

84 V. La Torre, E. Rambaldi, G. Masi, S. Nici, D. Ghezzi, M. Cappelletti and M. C. Bignozzi, Validation of Antibacterial Systems for Sustainable Ceramic Tiles, *Coatings*, 2021, **11**, 1409.

85 B. Lallo da Silva, M. P. Abuçafy, E. Berbel Manaia, J. A. Oshiro Junior, B. G. Chiari-Andréo, R. C. R. Pietro and L. A. Chiavacci, Relationship Between Structure And Antimicrobial Activity Of Zinc Oxide Nanoparticles: An Overview, *Int. J. Nanomed.*, 2019, **14**, 9395–9410.

86 W. Fan, Q. Sun, Y. Li, F. R. Tay and B. Fan, Synergistic mechanism of Ag^{+}–Zn^{2+} in anti-bacterial activity against Enterococcus faecalis and its application against dentin infection, *J. Nanobiotechnol.*, 2018, **16**, 10.

87 A. Gambardella, M. Berni, G. Graziani, A. Kovtun, A. Liscio, A. Russo, A. Visani and M. Bianchi, Nanostructured Ag thin films deposited by pulsed electron ablation, *Appl. Surf. Sci.*, 2019, **475**, 917–925.

88 A. Gambardella, M. Berni, A. Russo and M. Bianchi, A comparative study of the growth dynamics of zirconia thin films deposited by ionized jet deposition onto different substrates, *Surf. Coat. Technol.*, 2018, **337**, 306–312.